SUPPORTING INFORMATION

Chinese Journal of Structural Chemistry

In-situ Construction of Sulfur-doped g-C_3N_4/defective g-C_3N_4 Isotype Step-scheme Heterojunction for Boosting Photocatalytic H_2 Evolution

Jing Zou[1], Guodong Liao[1], Jizhou Jiang[1,2]*, Zhiguo Xiong[1], Saishuai Bai[1], Haitao Wang[1]*, Pingxiu Wu[3], Peng Zhang[4] and Xin Li[5]*

[1]*School of Environmental Ecology and Biological Engineering, School of Chemistry and Environmental Engineering, Key Laboratory of Green Chemical Engineering Process of Ministry of Education, Engineering Research Center of Phosphorus Resources Development and Utilization of Ministry of Education, Wuhan Institute of Technology, Wuhan 430205, China*

[2]*Key Laboratory of Rare Mineral, Ministry of Natural Resources, Geological Experimental Testing Center of Hubei Province, Wuhan 430034, China*

[3]*Semiconductor Electronic Special Gas of Hubei Engineering Research Center, Jingzhou, Hubei 434000, China*

[4]*State Centre for International Cooperation on Designer Low-Carbon & Environmental Materials (CDLCEM), School of Materials Science and Engineering, Zhengzhou University, Zhengzhou 450001, China*

[5]*Institute of Biomass Engineering, Key Laboratory of Energy Plants Resource and Utilization, Ministry of Agriculture and Rural Affairs, South China Agricultural University, Guangzhou 510642, China*

Corresponding authors. E-mail: 027wit@163.com (J. Jiang), wanghaitao@wit.edu.cn (H. Wang), xinli@scau.edu.cn (X. Li)

1. Physical Characterizations

The surface morphology and element composition analyses were examined by field emission scanning electron microscopy (FESEM, Gemini SEM 300, Germany Zeiss) and energy-dispersive X-ray spectroscope (EDX). The microstructures of all samples were examined by transmission electron microscopy (TEM) using a Tecnai G2 20 microscope operating at an acceleration voltage of 200 kV. The crystallographic structures were recorded on a Powder X-ray diffractometer (XRD, Bruker D8 ADVANCE diffractometer). The electronic structures and surface chemical components were analyzed by X-ray photoelectron spectroscopy (XPS, ESCALAB XI+-600W, Thermo Fisher Scientific). The surface area (BET) and pore size distributions (PSD) were recorded by N_2 adsorption- desorption isotherm on a surface analyzer (ASAP 2020 HD88, Micromeritics USA). The pore size distributions were calculated according to the Barrett-Joyner-Halenda (BJH) method from the branch of adsorption isotherm.

2. Photoelectrochemical Measurements

UV-VIS diffuse reflectance spectra of all materials were measured by a Carry5000 UV-vis spectrophotometer (Agilent) in the range of 300–700 nm. Transient fluorescence decay spectra and photoluminescence (PL) emission spectra of as-obtained photocatalysts were performed by an Edinburgh-FLS980 (England) spectrophotometer. Transient photocurrent responses (TPR) and Electrochemical impedance spectroscopy (EIS) measurements were evaluated on an electrochemical workstation (CHI660e Instruments) with a standard three-electrode photoelectrochemical cell. A Ag/AgCl electrode, a platinum-wire electrode and a potocatalyst-coated glassy carbon electrode (GCE, 3 mmin diameter) were employed as the reference, counter, and working electrodes, respectively. For thr working electrode preparation, 10 mg of as-prepared potocatalysts was mixed with 5 mL of deionized water, then 5 μL of the homogeneous suspension was pipetted onto an indium tin oxide (ITO) conductive glass. Particularly, the electrolytes required for TPR and EIS tests were 0.5 M Na_2SO_4 (pH = 6.7) and 5 mmol/L potassium ferricyanide solution, respectively. In addition, a 10 W xenon lamp (410–420 nm) was employed as the light source during TPR measurement.

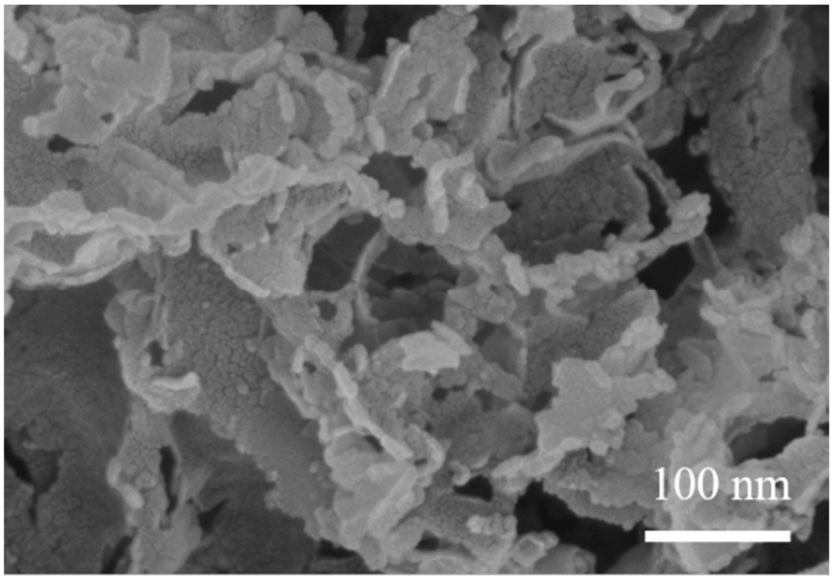

Figure S1. SEM image of g-C_3N_4.

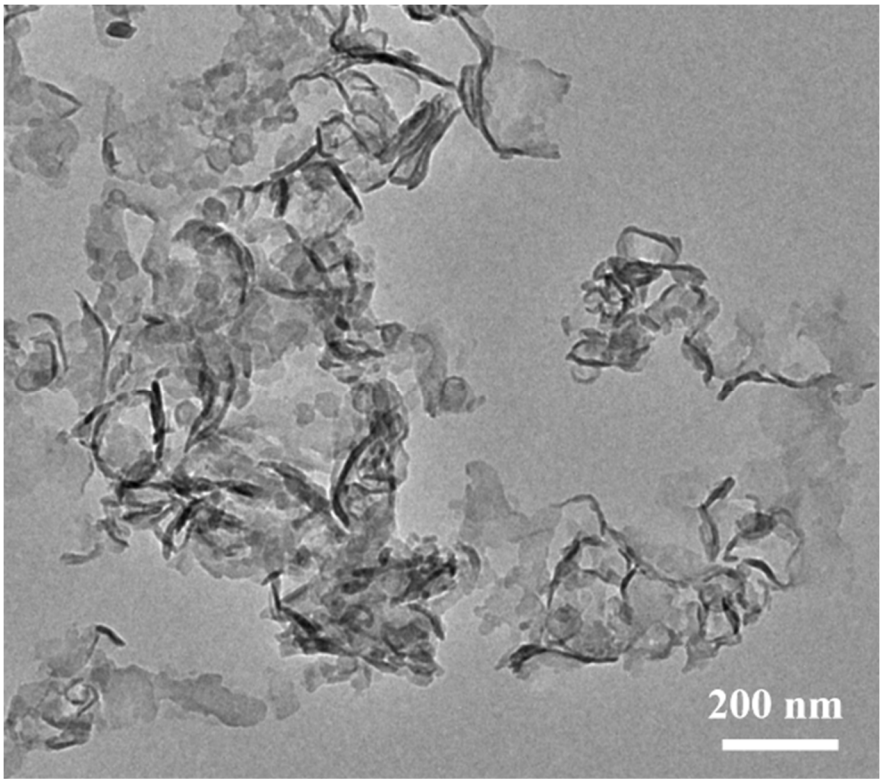

Figure S2. TEM image of g-C_3N_4.

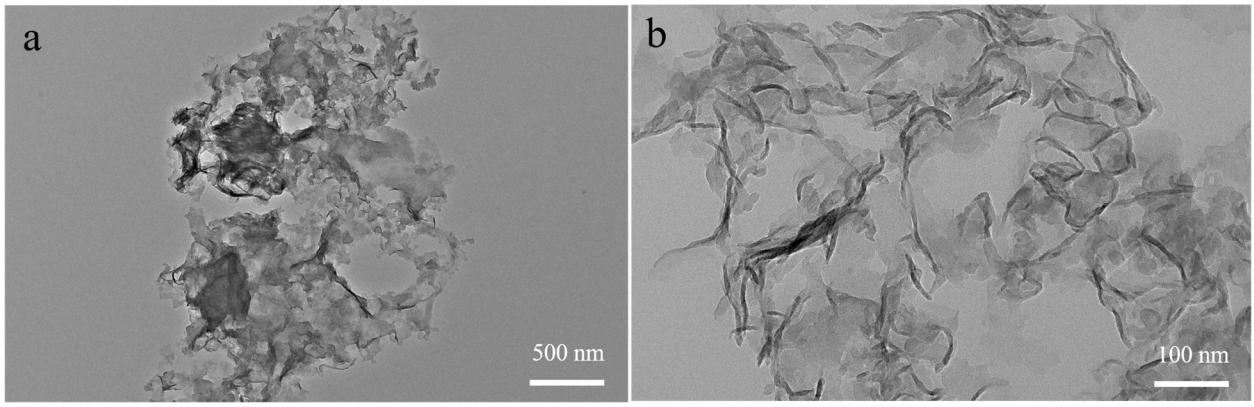

Figure S3. TEM images of S-g-C_3N_4-D.

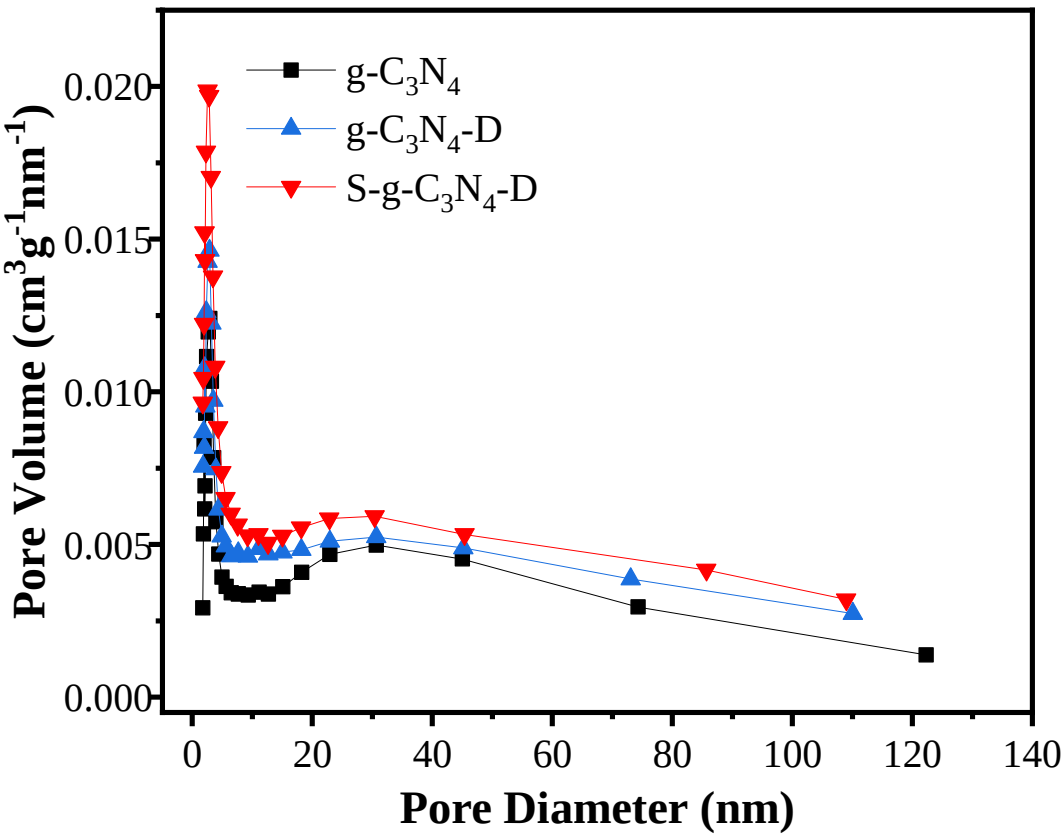

Figure S4. The pore size distribution curves of g-C_3N_4, g-C_3N_4-D, and S-g-C_3N_4-D.

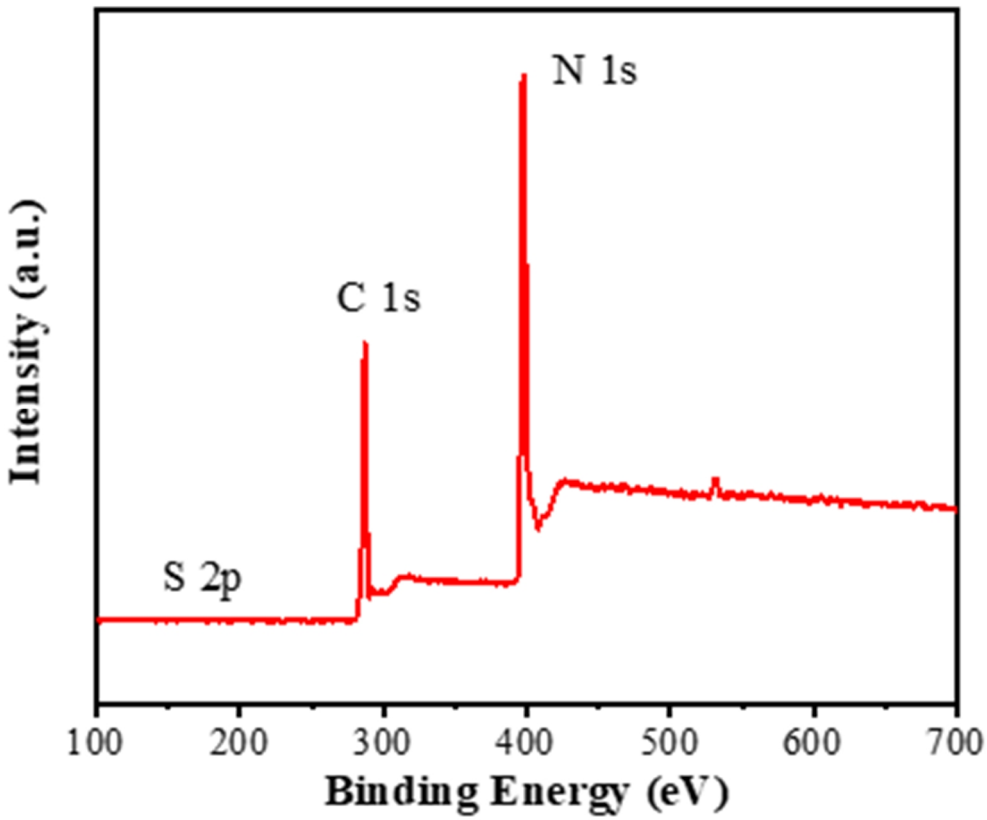

Figure S5. XPS survey spectrum of S-g-C_3N_4-D.

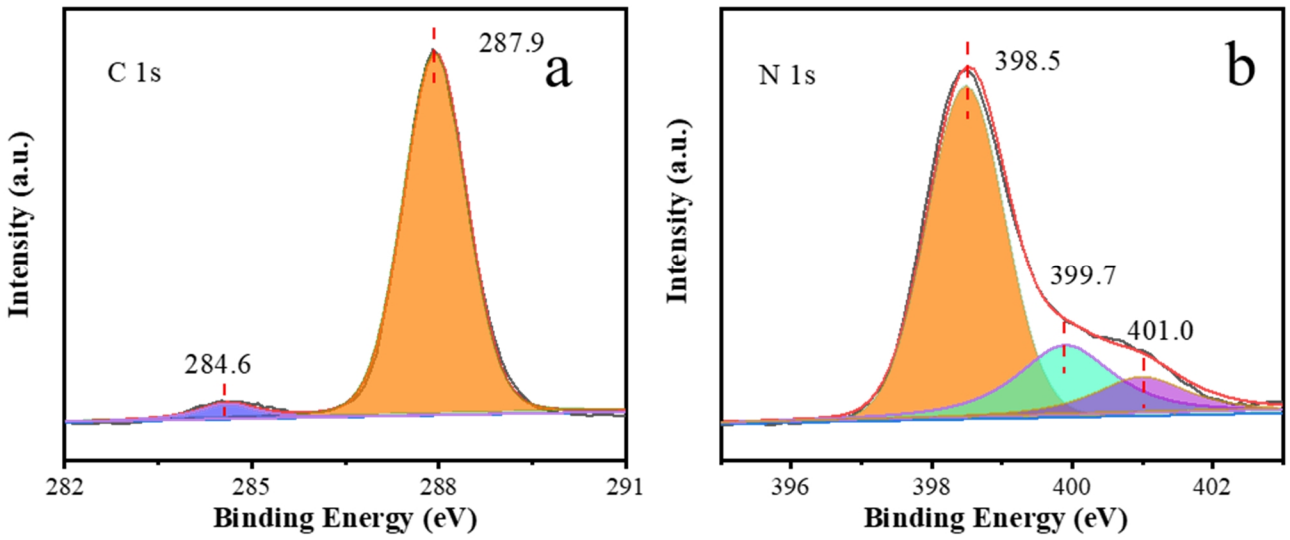

Figure S6. The high-resolution (a) C 1*s* and (b) N 1*s* spectra of S-g-C_3N_4-D.

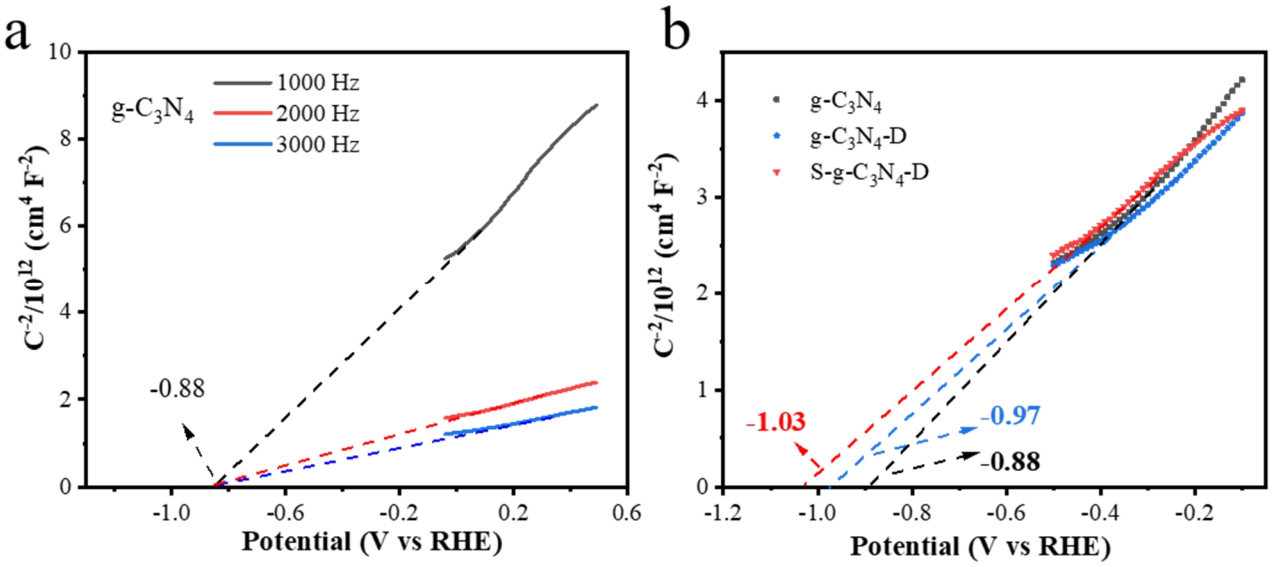

Figure S7. (a) Mott-Schottky plots of g-C_3N_4 obtained from different frequencies. (b) Mott-Schottky plots of g-C_3N_4, g-C_3N_4-D, and S-g-C_3N_4-D.

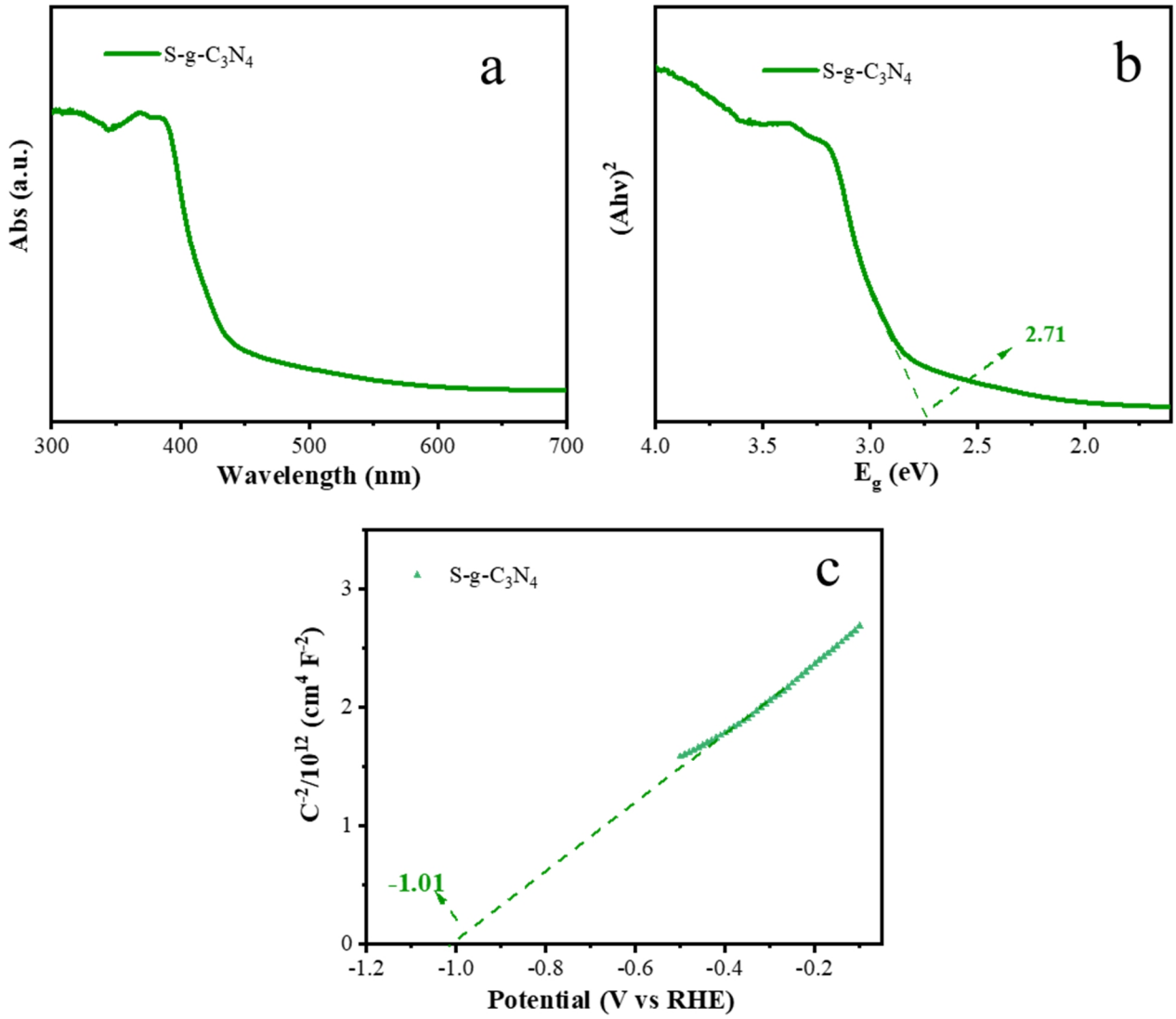

Figure S8. (a) UV-vis absorption spectrum and (b) the corresponding estimated energy gap of S-g-C_3N_4. (c) Mott-Schottky plot of S-g-C_3N_4.

Table S1. The BET Surface Areas, Total Pore Volumes and Average Pore Size of g-C_3N_4, g-C_3N_4-D and S-g-C_3N_4-D.

Samples	BET surface area (m^2/g)	Total pore volume (cm^3/g)	Average pore size (nm)
g-C_3N_4	96.78	0.60	2.13
g-C_3N_4-D	112.83	0.68	2.42
S-g-C_3N_4-D	135.74	0.72	2.58

Table S2. The XPS Results of g-C_3N_4, g-C_3N_4-D and S-g-C_3N_4-D.

Samples	Peak	Binding energy (eV)	Assignment	FWHM (eV)	Area (Arb. unit)	Peak areas ratio (%)
g-C_3N_4	C 1*s*	287.9	N–C=N	1.2	82973	98.3
		284.6	C–C	1.2	1447	2.7
g-C_3N_4-D		287.9	N–C=N	1.2	78370	93.3
		284.6	C–C	1.4	5663	6.7
S-g-C_3N_4-D		287.9	N–C=N	1.2	75129	95.1
		284.6	C–C	1.1	3871	4.9
g-C_3N_4	N 1*s*	398.5	N–C=N	1.2	150455	74.7
		399.7	N–$(C)_3$	1.1	28806	14.3
		401.0	-NH	1.1	22281	12.0
g-C_3N_4-D		398.5	N–C=N	1.2	136461	70.1
		399.7	N–$(C)_3$	1.3	30648	15.8
		401.0	-NH	1.4	27452	14.1
S-g-C_3N_4-D		398.5	N–C=N	1.3	129439	64.7
		399.7	N–$(C)_3$	1.4	43236	21.6
		401.0	-NH	1.4	27280	13.7
S-g-C_3N_4-D	S 2*p*	165.4	C–S–C	2.1	447	100

Table S3. The Comparisons of Photocatalytic H_2 Evolution Activities between S-g-C_3N_4-D and Other S-doped C_3N_4 Relevant Photocatalysts Previously Reported.

Photocatalyst	Amount of photocatalyst (mg)	Sacrificial reagent	Co-catalysts	Light source	H_2 Evolution ($\mu mol \cdot g^{-1} \cdot h^{-1}$)	Ref.
S-g-C_3N_4-D	**20**	**10 vol% of TEOA**	**3 wt% Pt**	**300 W Xe lamp (> 420 nm)**	**3110.1**	**This work**
PCNS	15	10 vol% of TEOA	2 wt% Pt	300 W Xe lamp (> 420 nm)	880.2	1
SCN1.0	50	10 vol% of TEOA	3 wt% Pt	300 W Xe lamp (> 400 nm)	141.9	2
MTCN-6	40	20 vol% of TEOA	1 wt% Pt	300 W Xe lamp (> 420 nm)	1511.2	3
SCCN0.1	50	10 vol% of TEOA	1 wt% Pt	150 W Xe lamp (> 420 nm)	1262.5	4
0.3S-CN	10	17 vol% of TEOA	1 wt% Pt	500 W Xe lamp (> 420 nm)	952	5
CoS_x/SCN	50	10 vol% of TEOA	0.75 wt% Pt	300 W Xe lamp (> 420 nm)	573.06	6
PSCN	20	20 vol% of TEOA	3 wt% Pt	300 W Xe lamp (> 400 nm)	1969	7
PCN-S-3	100	10 vol% of TEOA	1 wt% Pt	300 W Xe lamp (> 420 nm)	318	8
CNBS	20	10 vol% of TEOA	1 wt% Pt	150 W Xe lamp (> 420 nm)	2660	9
PCNS	15	10 vol% of TEOA	—	300 W Xe lamp (> 420 nm)	345	10
CoS_2@SCN	50	30 vol% of TEOA	—	500 W Xe lamp (> 420 nm)	223.6	11
S-Cu_2O/g-C_3N_4	100	10 vol% of TEOA	0.38 wt% Pt	300 W Xe lamp (> 400 nm)	240.8	12
NS-GC	10	10 vol% of TEOA	3 wt% Pt	400 W Xe lamp (> 420 nm)	310.63	13
Mo/S/g-C_3N_4	25	10 vol% of CH_3OH	-	300 W Xe lamp (> 420 nm)	294	14
2D-SCN	50	5 vol% of TEOA	1 wt% Pt	140 W Xe lamp (> 420 nm)	2548	15
In_2O_3/SCN	20	10 vol% of TEOA	-	300 W Xe lamp (> 420 nm)	93	16

Table S4. The Fitted Fluorescence Lifetimes, the Average Lifetimes and Corresponding Amplitudes of Photoinduced Charge Carriers in g-C_3N_4, g-C_3N_4-D and S-g-C_3N_4-D

Samples	Lifetime, τ (ns)	Rel (%)	τ_{Avg} (ns)
g-C_3N_4	τ_1 = 1.566	A_1 = 72.56	4.190
	τ_2 = 6.143	A_2 = 27.44	
g-C_3N_4-D	τ_1 = 1.401	A_1 = 70.26	4.602
	τ_2 = 6.288	A_2 = 29.74	
S-g-C_3N_4-D	τ_1 = 1.692	A_1 = 65.03	5.215
	τ_2 = 6.837	A_2 = 34.97	

SUPPLEMENTARY REFERENCES

(1) Bai, J. R.; Zhou, P.; Xu, P.; Deng, Y. Y.; Zhou, Q. F. Synergy of dopants and porous structures in graphitic carbon nitride for efficient photocatalytic H_2 evolution. *Ceram. Int.* **2021**, 47, 4043–4048.

(2) Fei, T.; Qin, C. C.; Zhang, Y. W.; Dong, G. M.; Wang, Y. Y.; Zhou, Y. M.; Cui, M. H. A 3D peony-like sulfur-doped carbon nitride synthesized by self-assembly for efficient photocatalytic hydrogen production. *Int. J. Hydrogen Energy* **2021**, 46, 20481–20491.

(3) Wang, H.; Bian, Y. R.; Hu, J. T.; Dai, L. M. Highly crystalline sulfur-doped carbon nitride as photocatalyst for efficient visible-light hydrogen generation. *Appl. Catal. B: Environ.* **2018**, 238, 592–598.

(4) Tian, H.; Zhang, X.; Bu, Y. Sulfur- and carbon-codoped carbon nitride for photocatalytic hydrogen evolution performance improvement. *ACS Sustain. Chem. Eng.* **2018**, 6, 7346–7354.

(5) Long, D.; Wang, L.; Cai, H. Y.; Rao, X.; Zhang, Y. P. Sulfur doped carbon-rich g-C_3N_4 for enhanced photocatalytic H_2 evolution: morphology and crystallinity effect. *Catal. Lett.* **2020**, 150, 2487–2496.

(6) Shen, Q. H.; Bibi, R.; Wei, L. F.; Hao, D. D.; Li, N. X.; Zhou, C. Well-dispersed CoS_x nanoparticles modified tubular sulfur doped carbon nitride for enhanced photocatalytic H_2 production activity. *Int. J. Hydrogen Energy* **2019**, 44, 14550–14560.

(7) Hou, P.; Meng, X. L.; Li, L.; Sun, T. H. P, S Co-doped g-C_3N_4 isotype heterojunction composites for high-efficiency photocatalytic H_2 evolution. *J. Alloys Compd.* **2020**, 827, 154259.

(8) Lin, Q. C.; Li, Z. S.; Lin, T. J.; Li, B. L.; Liao, X. C.; Yu, H. Q.; Yu, C. L. Controlled preparation of P-doped g-C_3N_4 nanosheets for efficient photocatalytic hydrogen production. *Chin. J. Chem. Eng.* **2020**, 28, 2677–2688.

(9) Babu, P.; Mohanty, S.; Naik, B.; Parida, K. Synergistic effects of boron and sulfur co-doping into graphitic carbon nitride framework for enhanced photocatalytic activity in visible light driven hydrogen generation. *ACS Adv. Energy Mater.* **2018**, 1, 5936–5947.

(10) Zhou, Y.; Lv, W. H.; Zhu, B. L.; Tong, F.; Pan, J. L.; Bai, J. R.; Zhou, Q. F.; Qin, H. F. Template-free one-step synthesis of g-C_3N_4 nanosheets with simultaneous porous network and S-doping for remarkable visible-light-driven hydrogen evolution. *ACS Sustain. Chem. Eng.* **2019**, 7, 5801–5807.

(11) Wang, L.; Geng, X. L.; Zhang, L.; Liu, Z. H.; Wang, H.; Bian, Z. Y. Effects of various alcohol sacrificial agents on hydrogen evolution based on CoS_2@SCN nanomaterials and its mechanism. *Chemosphere* **2022**, 286, 131558.

(12) Gu, Y. H.; Bao, A.; Zhang, X. Y.; Yan, J. H.; Du, Q.; Zhang, M.; Qi, X. W. Facile fabrication of sulfur-doped Cu_2O and g-C_3N_4 with Z-scheme structure for enhanced photocatalytic water splitting performance. *Mater. Chem. Phys.* **2021**, 266, 124542.

(13) Das, B.; Gogoi, D.; Devi, M.; Dhar, S. S.; Peela, N. R. Synergistic effect of metal complex and dual doped graphitic carbon nitride for superior photocatalytic hydrogen evolution. *Energy Fuels* **2021**, 35, 15223–15233.

(14) Li, Y. Y.; Zhu, S. L.; Liang, Y. Q.; Li, Z. Y.; Wu, S. L.; Chang, C. T.; Luo, S. Y.; Cui, Z. D. One-step synthesis of Mo and S co-doped porous g-C_3N_4 nanosheets for efficient visible-light photocatalytic hydrogen evolution. *Appl. Surf. Sci.* **2021**, 536, 147743.

(15) Lv, H. Q.; Huang, Y.; Koodali, R. T.; Liu, G. M.; Zeng, Y. B.; Meng, Q. G.; Yuan, M. Z. Synthesis of sulfur-doped 2D graphitic carbon nitride nanosheets for efficient photocatalytic degradation of phenol and hydrogen evolution. *ACS Appl. Mater. Interfaces* **2020**, 12, 12656–12677.

(16) Zhou, P.; Meng, X. L.; Sun, T. H. Facile fabrication of In_2O_3/S-doped g-C_3N_4 heterojunction hybrids for enhanced visible-light photocatalytic hydrogen evolution. *Mater. Lett.* **2019**, 261, 127159.